Case Studies in Chemical and Environmental Engineering 11 (2025) 101081

Contents lists available at ScienceDirect

Case Studies in Chemical and Environmental Engineering

journal homepage: www.sciencedirect.com/journal/case-studies-in-chemical-and-environmental-engineering

Case Report

Water management and conductivity studies in novel polymer zirconium-based membranes for PEM fuel cells

Tallah Magdi Ahmed [a], Amani Al Othman [b,c,*], Abdulrahim Shamayleh [d], Muhammad Tawalbeh [e,f]

[a] Engineering Systems Management Graduate Program, American University of Sharjah, PO. Box 26666, Sharjah, United Arab Emirates
[b] Department of Chemical and Biological Engineering, American University of Sharjah, PO. Box 26666, Sharjah, United Arab Emirates
[c] Energy, Water and Sustainable Environment Research Center, American University of Sharjah, PO. Box 26666, Sharjah, United Arab Emirates
[d] Department of Industrial Engineering, American University of Sharjah, PO. Box 26666, Sharjah, United Arab Emirates
[e] Sustainable and Renewable Energy Engineering Department, University of Sharjah, PO. Box 27272, Sharjah, United Arab Emirates
[f] Sustainable Energy & Power Systems Research Centre, RISE, University of Sharjah, P.O. Box 27272, Sharjah, United Arab Emirates

ARTICLE INFO

Keywords:
Zirconium silicate
PVDF
Composite membranes
Water management
Proton conduction
PEM fuel cells

ABSTRACT

Proton exchange membrane fuel cells (PEMFCs) are among the promising alternatives for clean energy generation, especially when hydrogen is the fuel used. Their operation is still faced with several challenges, and one of them is water accumulation in the cathode compartment. If PEMFCs are operated at temperatures above the boiling point of water, a significant obstacle would be eliminated due to the formation of water in the vapor phase. This prevents water from accumulating in the liquid phase which causes flooding. Therefore, this work aims to develop a novel composite membrane based on zirconium silicate ($ZrSiO_4$) and Polyvinylidene fluoride (PVDF) for such high-temperature operation. The composite membrane was synthesized using solution casting, and its structural and chemical properties were characterized using thermogravimetric analysis (TGA), Fourier-transform infrared spectroscopy (FTIR), X-ray diffraction (XRD), and scanning electron microscopy (SEM) techniques. The $ZrSiO_4$/PVDF membrane demonstrated a maximum proton conductivity of 2.14×10^{-3} S/cm at room temperature with 8 wt% $ZrSiO_4$, along with a water uptake value of 43.85 %. Consequently, when tested above the boiling point of water, the membrane exhibited a high conductivity of 2.13×10^{-3} S/cm at 105 °C. The results suggest the suitability of such zirconium silicate-based composite membranes for fuel cell applications operating above the boiling point of water.

1. Introduction

Energy plays a crucial role in our daily lives, starting from its production and extending through to reach the last step of utilization. Nowadays, with the growing energy demand, the world's urge to explore green energy alternatives that can effectively substitute the existing sources has increased [1]. This is because transitioning to green energy solutions can significantly reduce greenhouse gas emissions, enhance energy security, and foster a cleaner, more sustainable environment, making it easier to align with the global net zero and sustainability goals [2]. In this context, electrochemical devices have emerged as key technologies in the quest for sustainable energy solutions, enabling the storage, conversion, and efficient use of renewable energy sources. These devices include supercapacitors, batteries, and fuel cells [3]. Among these, fuel cells stand out as a promising option for efficient energy conversion, offering notable advantages, such as high efficiency, reliable operation, and consistent performance across various scales [4]. Moreover, fuel cells are employed in various applications ranging from power generation to water treatment [5,6]. Typically, fuel cells are categorized into six types depending on their electrolytes: proton exchange membrane (PEM) fuel cell, alkaline fuel cell (AFC), direct methanol fuel cell (DMFC), phosphoric acid fuel cell (PAFC), molten carbonate fuel cell (MCFC), and solid oxide fuel cell (SOFC) [7,8]. According to a report by Fortune Business Insights in 2021, the global market is currently dominated by the PEM fuel cell segment by 70.5 %. This strong preference for PEMFCs is driven by their distinctive advantages compared to other fuel cell varieties [9]. Key benefits, such as the flexibility in fuel inputs, compact and lightweight design,

* Corresponding author. Department of Chemical and Biological Engineering, American University of Sharjah, PO. Box 26666, Sharjah, United Arab Emirates.
E-mail address: aalothman@aus.edu (A. Al Othman).

https://doi.org/10.1016/j.cscee.2024.101081
Received 12 October 2024; Received in revised form 20 December 2024; Accepted 23 December 2024
Available online 24 December 2024
2666-0164/© 2024 The Author(s). Published by Elsevier Ltd. This is an open access article under the CC BY-NC-ND license (http://creativecommons.org/licenses/by-nc-nd/4.0/).

cost-effectiveness, and durability of the electrolyte, have been essential in accelerating its adoption and market growth [10]. As a result, PEMFCs have been used in different fields of applications, such as transportation [11–13], military [14], marine applications [15], portable electronics [16], etc. In terms of structure, PEMFC comprises two electrodes, namely an anode and a cathode, where oxidation and reduction reactions occur, respectively. Moreover, the electrolyte employed in this fuel cell type is a polymer electrolyte membrane, which is positioned between the two electrodes. It plays an important role in facilitating the transmission of the H^+ ions for reduction to water and providing electronic insulation as well as separation of reactant gases [17–20].

When hydrogen is used as a fuel in PEMFCs, the primary byproduct is water in liquid form. However, as the cell operates, water tends to accumulate at the cathode, leading to a phenomenon known as "*cell flooding*" [21]. This accumulation impairs gas diffusion and reduces the overall efficiency and performance of the fuel cell. Therefore, in order to address this challenge, operating at high temperatures is required, which facilitates the elimination of the accumulated water in the form of vapor. Moreover, Nafion, the most widely used material in proton exchange membranes, was pioneered by E.I. DuPont de Nemours and Company in the 1960s. It was developed to fulfill the need for a durable cation exchange membrane in the electrochemical production of chlorine and sodium hydroxide, particularly within the chlor-alkali industry [22]. It consists of a perfluorinated aliphatic structure that forms the backbone, accompanied by side chains linked with ether that terminate in sulfonated cation exchange sites, resembling Teflon membranes [23, 24]. However, despite its widespread use, there are intrinsic limitations associated with its performance as a membrane. One of these limitations is that the Nafion membrane is expensive, which adds to the capital cost of the fuel cell system. Nafion also tends to degrade as it operates at temperatures higher than 80 °C [22]. As a result, the scientific community has been continuously engaged in exploring new materials to overcome the limitations of Nafion-based membranes and to improve their performance and composite membranes for high temperature fuel cells were reported [25–28]. The proposed work explores a novel membrane combining Polyvinylidene fluoride (PVDF) polymer and Zirconium silicate to address these challenges. PVDF is a fluoropolymer known for its low toxicity, chemical inertness, and thermal stability [29]. It is also highly hydrophobic, necessitating the incorporation of additives to improve its hydrophilicity for proton exchange membranes [30].

Zirconium-based materials have emerged as promising candidates due to their high thermal stability, mechanical strength, and chemical resistance, which address the inherent limitations of conventional Nafion membranes [31]. Nevertheless, a variety of zirconium-based materials have been explored in the literature. For instance, a study by Tawalbeh et al. [32] explored the development of Nafion-free membranes using zirconium silicate, lignin, and ionic liquids. It demonstrated significant enhancement in proton conductivity when lignin was incorporated, increasing the conductivity by two orders of magnitude. Zirconium silicate, also known as Zircon, is known for its high mechanical and thermal stability, as well as its good ion exchange capacity [33]. In this context, it is worth mentioning that Zircon distinguishes itself from Zirconia in critical ways. While Zirconia exhibits inherent electrical conductivity, zirconium silicate does not demonstrate that [34]. Instead, it possesses evident hydrophilic properties, which are in turn, required for proton hopping in proton exchange membranes. Its hydrophilicity facilitates water retention and hydrogen bonding within the membrane, which enables the transport of protons (proton conduction) [35]. The material's negative surface charge further contributes to enhancing proton conductivity by enabling the formation of hydration shells around ionic species, which promotes proton mobility [36]. Studies have demonstrated the potential of zirconium silicate in improving membrane performance. Similarly, complementary studies have explored other zirconium-based materials. For instance, Al-Othman et al. [37] developed a composite membrane incorporating zirconium phosphate, MXene, and ionic liquids into a porous PTFE polymer, achieving high proton conductivity 10^{-2} S/cm at 145 °C, with thermal stability confirmed by thermogravimetric analysis (TGA) analysis. The research highlights the potential of zirconium-based materials to overcome the inherent limitations of Nafion. Their hydrophilicity, ion exchange capacity, and thermal stability make them ideal for addressing challenges in high-temperature PEMFC operations. The ongoing development of PVDF-zirconium silicate membranes, supported by water uptake and other characterization studies, underscores their potential to replace existing membranes and advance the field of fuel cell technology.

2. Experimental setup and method

2.1. Materials

The PVDF pellets, used in this study, were purchased from Sigma Aldrich, USA, and were employed without any further chemical modification or crosslinking. Polymers crosslinking is described in the literature along with membrane casting [38]. Silicic acid (H_2SiO_4) was also procured from Sigma Aldrich, USA. Zirconium oxychloride octahydrate ($ZrOCl_2{\cdot}8H_2O$), meeting ACS 98 % standards, was obtained from Sigma-Aldrich, China. Furthermore, dimethylacetamide (DMaC) solvent with a purity of $\geq$99 % was sourced from Sigma Aldrich, Germany, and was utilized without any additional purification or alteration.

2.2. Membrane synthesis

The process of membrane synthesis starts by combining a 1 M solution of zirconium oxychloride and silicic acid, followed by stirring the mixture at 200 rpm for 30 minutes at room temperature, as explained by Pandey et al. [39]. The solution was then left to age for 24 hours, resulting in the formation of a white precipitate, Zirconium silicate, as illustrated in Eq. (1). This precipitate was filtered to obtain a sol-gel form.

$$ZrOCl_{2\,(aq)} + H_2SiO_{4\,(aq)} \rightarrow ZrSiO_{4\,(s)} + 2HCl_{\,(aq)} \quad (1)$$

In the next step, 0.5 wt% of the produced $ZrSiO_4$ was dissolved in DMac and stirred for 30 minutes at 70 °C and 200 rpm to ensure complete gel dissolution. Subsequently, 10 wt% of PVDF pellets were added to the mixture, and the stirring continued for an additional 30 minutes at 70 °C, resulting in a thicker and more viscous solution. The solution casting method, as illustrated by Lee et al. [40], was employed to develop the membranes, where the blend was poured onto a Petri dish and left to desiccate at 90 °C for 2–3 hours until a peelable membrane was formed. Additionally, to ensure consistent membrane thickness and eliminate it as a variable, each membrane was cast using Petri dishes of identical diameter (100 mm), with a fixed matrix amount of 6 g per membrane. The mean and standard deviation of membrane thickness across samples were calculated to be 0.00478 and 0.000176 cm, respectively, confirming uniformity. This process was repeated for the different amounts of $ZrSiO_4$ to enable comprehensive experimentation and analysis, enhancing the robustness and versatility of the synthesized membranes. Fig. 1 illustrates the schematic representation of the experimental process.

2.3. Membrane characterization

The characterization of the synthesized membranes is important to understand their structural, chemical, and electrochemical properties. Various techniques were employed to evaluate key properties, such as proton conductivity, water uptake, thermal stability, and molecular composition. These analyses provide valuable insights into the performance and potential applications of the membranes, particularly in

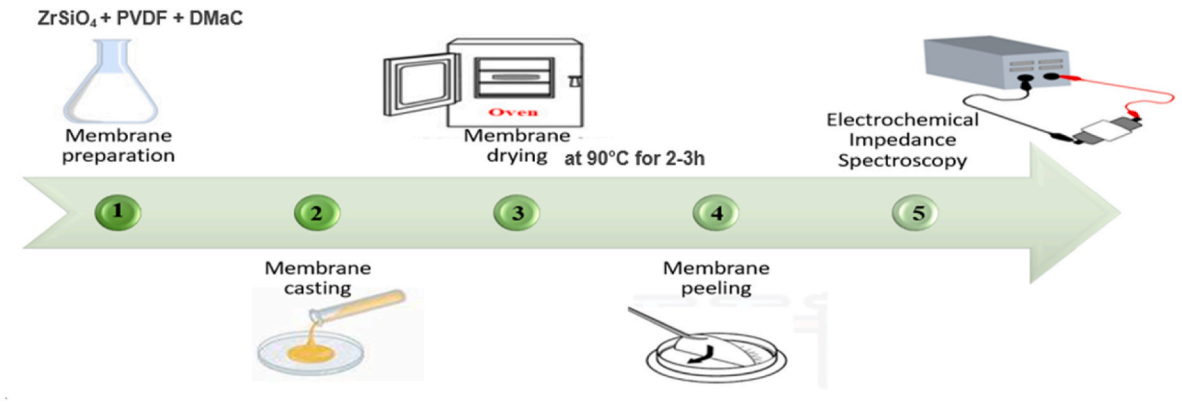


Fig. 1. Schematic diagram of the experimental procedure.

high-temperature fuel cell systems.

2.3.1. Electrochemical impedance spectroscopy

The proton conductivities of the produced membranes were assessed through electrochemical impedance spectroscopy (EIS). To begin, a membrane sample was prepared by cutting it and securely positioning it within the fuel simulation cell. Impedance data were then gathered across a frequency range of 0.0003–7 MHz using the Bio-Logic SP-200 Potentiostat and ITS instruments. The Nyquist plots obtained from these measurements were analyzed utilizing EC-Lab software (Version 11.10) to ascertain the resistances of the membranes. Subsequently, these resistance values were utilized in Eq. (2) to calculate the proton conductivity (σ) [31].

$$\sigma = \frac{t}{Z \bullet A} \tag{2}$$

where t is the membrane sample thickness, Z is the sample impedance and A is the cross-sectional area of the simulation cell.

2.3.2. Water uptake

The membranes in their dry state were weighed and placed in deionized water at 80 °C for a period of 24 hours. The water uptake (WU) was determined using Eq. (3):

$$WU(\%) = \frac{w_h - w_d}{w_d} \times 100\% \tag{3}$$

where w_d represents the membranes' weight prior to water absorption, and w_h is the weight after the 24-h water immersion.

2.3.3. Thermogravimetric analysis

The TGA was used to assess the membranes' thermal stability. The PerkinElmer TGA 4000 Thermogravimetric Analyzer was used to conduct the analysis. The samples were heated under nitrogen (N_2) at a rate of 20 °C/min. The temperature range that the samples were subjected to was 25–700 °C.

2.3.4. Fourier transform infrared spectroscopy

Fourier transform infrared spectroscopy (FTIR) was utilized to gain insights into the molecular composition of the membranes by measuring the absorption of infrared light across different frequencies. To conduct this analysis, a PerkinElmer instrument operated over a wavelength range of 399–4000 cm^{-1} was utilized. The purpose was to identify the various functional groups and chemical bonds present within the membrane structure.

2.3.5. X-ray diffraction

X-ray diffraction (XRD) relies on Bragg's law to explain the scattering of X-rays in crystal lattices. In this technique, a monochromatic X-ray beam is directed at a crystalline sample, and the resulting diffraction pattern is captured. For this analysis, the Bruker D8 Advanced system with a 1-D detector and scintillation point detector was utilized to obtain detailed insights into the sample's crystal structure.

2.3.6. Scanning electron microscopy and energy dispersive X-ray spectroscopy analysis

Scanning Electron Microscopy (SEM) uses a high-energy electron beam to scan a sample's surface, generating secondary and backscattered electrons as well as X-rays. This allows for high-resolution imaging and analysis of surface features. In this study, SEM analysis was performed using the Tescan VEGA XMU device, with an Oxford Instruments X-Max 50 SSD detector and LaB6 filament. The technique is instrumental in observing the membrane's surface morphology, helping to evaluate its structural properties and potential for fuel cell applications. Energy dispersive X-ray spectroscopy analysis (EDX) was also performed on the samples using the same machine to find the elemental composition.

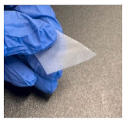
3. Results and discussion

In this section, the results based on the effect of $ZrSiO_4$ on the proton conductivity of PVDF membranes are discussed, in addition to the membrane characterization findings.

3.1. Effect of $ZrSiO_4$ on PVDF membranes' proton conductivity at room temperature

To investigate the impact of $ZrSiO_4$ nanoparticles on the proton conductivity of PVDF membranes, a series of membrane samples were developed with varying concentrations ranging from 0 to 10 wt% of $ZrSiO_4$. These samples were tested via EIS. Proton conductivity measurements were conducted at room temperature. The resistance of the membrane was determined by extrapolating the horizontal axis in the region of high frequency and fitting it using models in the EC lab software. The resulting proton conductivity values for these membranes are reported in S/cm. For each membrane, replicate measurements were conducted to ensure data reliability and standard deviations were calculated to assess variability. The pure PVDF membrane exhibited a proton conductivity of 1.8×10^{-4} S/cm. Upon adding $ZrSiO_4$, the $ZrSiO_4$/PVDF composite membrane exhibited a substantial increase in proton conductivity. Particularly, as described in Table 1, the membrane with an 8 % $ZrSiO_4$ content showcased the best proton conductivity at 2.145×10^{-3} S/cm, which means that the conductivity increased by almost one order of magnitude. The standard deviation for the proton conductivity of this sample was calculated to be 3.536×10^{-6} S/cm, indicating minimal variability across replicates. The increase in proton conductivity can be basically attributed to the enhanced hydrophilic

Table 1
Resistance and proton conductivities of different membranes synthesized in this work. Note: This results in a total of two replicates for each measurement.

No.	$ZrSiO_4$ (wt. %)	Z (Ω)	σ (S/cm)	St. Deviation (S/cm)	Membrane
1	0 %	43.85	1.83×10^{-4}	4.243×10^{-6}	
2	1.5 %	15.09	4.79×10^{-4}	1.273×10^{-5}	
3	3 %	12.22	6.3×10^{-4}	2.333×10^{-5}	
4	8 %	7.991	2.145×10^{-3}	3.536×10^{-6}	

properties introduced by incorporating $ZrSiO_4$. Based on the SEM analysis in section 3.3.5, the nanoparticles created micro- and nano-scale channels within the PVDF polymer matrix, as observed in the SEM images. These channels appear as the result of the introduction of $ZrSiO_4$. Further changes appear as the formation of interconnected spherical particles and increased surface roughness for the tested membrane. The hydrophilic nature of $ZrSiO_4$ attracts and retains water molecules, presumably by hydrogen bonding, within these channels leading to enhanced water retention. The presence of more water molecules improves the membrane's hydration and offers more pathways that facilitate proton conduction. Proton conduction is known to take place via mechanisms like proton hopping. Water retention ensures the presence of hydrogen-bonded networks, to facilitate this mechanism, where protons can "hop" from one water molecule to another. In this way, $ZrSiO_4$ inclusion directly contributes to the creation of multiple proton conduction paths, thus, increasing the membrane's water uptake increases proton conduction. Nevertheless, it is important to note that the 10 % $ZrSiO_4$ membrane was very fragile and broke easily, making it difficult to measure its conductivity. The mechanical stability and durability of the membranes are crucial factors. Hence, the most achievable increase was up to 8 %. The Nyquist plot of 8 wt% $ZrSiO_4$ had an intersection at 7.991 Ω with the x-axis. To fit the plot, EC-Lab software (V11.1) was used. The effect of increasing $ZrSiO_4$ content in the PVDF matrix can be noticed in Fig. 2. To further enhance the performance of $ZrSiO_4$/PVDF composite membranes while overcoming mechanical fragility at higher concentrations, such as 10 %, a few strategies are to be considered. One approach could be optimizing the $ZrSiO_4$ content, focusing on the 8 % concentration where proton conductivity is maximized without compromising the mechanical stability. Additionally, incorporating flexible or reinforcing polymers, such as polyether sulfone (PES), PDMS polymer or carbon-based nanomaterials (e.g., graphene oxide) can increase mechanical strength while maintaining or even improving proton conductivity. This combination could offer a balanced enhancement in both conductivity and durability, ensuring more reliable membrane performance for high-temperature applications.

3.2. Conductivity of the best-performing membranes at elevated temperatures

The examination of the best-performing membrane (8 wt% $ZrSiO_4$) under different high-temperature settings aims to understand how its proton conductivity changes in elevated operational conditions. High-temperature operation is necessary to address water management challenges in fuel cells and flooding [41]. Operating above water's boiling point helps vaporize accumulated water during fuel cell operation, making its removal easier. The membrane underwent thorough evaluation across temperatures ranging from 25 to 145 °C. Proton conductivities were carefully recorded and tabulated in Table 2 and Fig. 3. A noticeable fluctuation in proton conductivity is observed across the temperature range, indicating the dynamic relationship between temperature variations and proton conduction in the membrane. There is a significant peak in proton conductivity observed at 55 °C and 105 °C, where the membrane exhibited high values of 2.23×10^{-3} S/cm and 2.13×10^{-3} S/cm, respectively. However, since the objective is to

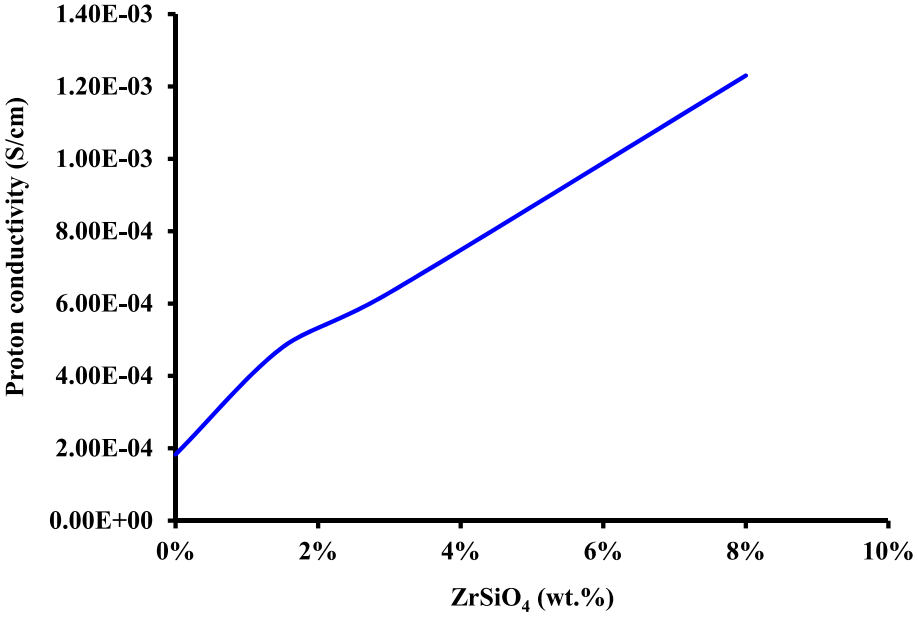


Fig. 2. Proton conductivity of different wt.% of $ZrSiO_4$ in the PVDF matrix.

Table 2
Water uptake percentages of the synthesized membranes.

Membrane	Water uptake (%)	St. Deviation (%)	Ref.
0 wt% $ZrSiO_4$/PVDF	11.60	0.24	This work
1.5 wt% $ZrSiO_4$/PVDF	23.03	1.17	This work
3 wt% $ZrSiO_4$/PVDF	23.70	1.22	This work
8 wt% $ZrSiO_4$/PVDF	43.85	1.27	This work
Nafion-117	29.2	–	[39]
Nafion/H_3PO_4@S1-15	28.8	–	[44]
MXene/Glycerol/PVDF	39	–	[29]
Si-PWA/PVDF	30.3	–	[45]

operate at high temperatures, operating at 105 °C will be considered. This test highlights the membrane's ability to perform well under elevated temperatures, indicating its potential for high-temperature applications.

3.3. Characterization results

3.3.1. Water uptake

The WU analysis was conducted to investigate the membrane properties, a critical factor influencing fuel cell performance. In the analysis, membranes were subjected to a controlled drying process at 100 °C for 2 hours to remove any existing moisture and standardize their initial dry weight measurement. This step ensures consistency and accuracy in subsequent measurements. Following the drying process, the membranes were immersed in distilled water at a temperature of 25 °C for 24 hours allowing them to reach equilibrium and ensuring that maximum water absorption is achieved. Then, the membranes were reweighed to determine their hydrated weights, using Eq. (3), as specified in the methodology. To ensure the reliability of the data, additional replicate measurements for the WU were conducted on each membrane, and the resulting standard deviations were calculated to assess the consistency of the results.

As seen in Table 2, the summary of the obtained results reveals significant variations in WU percentages among different membrane compositions. The pure PVDF membrane exhibited a relatively low WU of 11.6 %. However, upon incorporating $ZrSiO_4$ into the membrane matrix, a substantial increase in WU was observed, with the highest value of 43.85 % recorded for membranes containing 8 wt% $ZrSiO_4$. This enhancement in WU suggests that $ZrSiO_4$ improves the membrane's hydrophilicity due to the presence of Si–OH bonds, which strengthen interactions with water molecules. Furthermore, similar to the findings of SnO_2-doped membranes [42,43], the inclusion of $ZrSiO_4$ enhanced proton conductivity values, with the highest proton conductivity observed in the $ZrSiO_4$ membranes, likely due to improved water retention and hydrogen bonding. However, the difference in water retention trends between SnO_2 and $ZrSiO_4$ is attributed to the denser structure of SnO_2 nanoparticles, which restrict water molecule movement and block hydrophilic channels, reducing water absorption. In contrast, $ZrSiO_4$'s Si–OH bonds facilitate stronger interactions with water, enhancing water retention. These results align with literature that shows how adding inorganic nanoparticles like SnO_2 enhances proton conductivity by providing additional proton transport pathways, even with reduced water absorption, and suggest the promising potential of zirconium-based materials for high-temperature PEMFC applications [31]. When comparing the membrane with other developed membranes, it stands as a potential competitor in terms of WU and enhanced water retention properties.

3.3.2. Thermogravimetric analysis

The thermal stability of both pure PVDF and 8 wt% $ZrSiO_4$ membranes was assessed using thermogravimetric analysis under a controlled nitrogen supply, employing a heating rate of 20 °C/min within a temperature range of 25–700 °C. As shown in Fig. 4, an initial minor weight loss of approximately 2 % was noted at temperatures below 200 °C, attributed to the escape of bound water molecules from the membrane structure. The degradation behavior of the 8 wt% $ZrSiO_4$ membrane exhibited a multi-phase pattern. The first degradation phase, occurring within the temperature range of 300–450 °C, is indicative of the potential degradation of Zr–Si–OH bonds within the membrane structure. Subsequently, a second degradation phase spanning 450–500 °C was observed, corresponding to the degradation temperature range of PVDF as reported in the literature [46]. The final phase, characterized by a sharp decline in weight, culminated in complete membrane degradation at approximately 600 °C. Conversely, the thermal degradation of the pure PVDF membrane manifested in two distinct phases. The initial degradation phase, spanning 440–500 °C, marked the onset of significant weight loss, followed by a secondary phase extending from 510 to 680 °C, where substantial membrane degradation occurred. Notably, the inclusion of zirconium silicate into the membrane matrix resulted in reduced thermal stability, as evidenced by the observed degradation limit of 600 °C. This contrasts with the pure PVDF

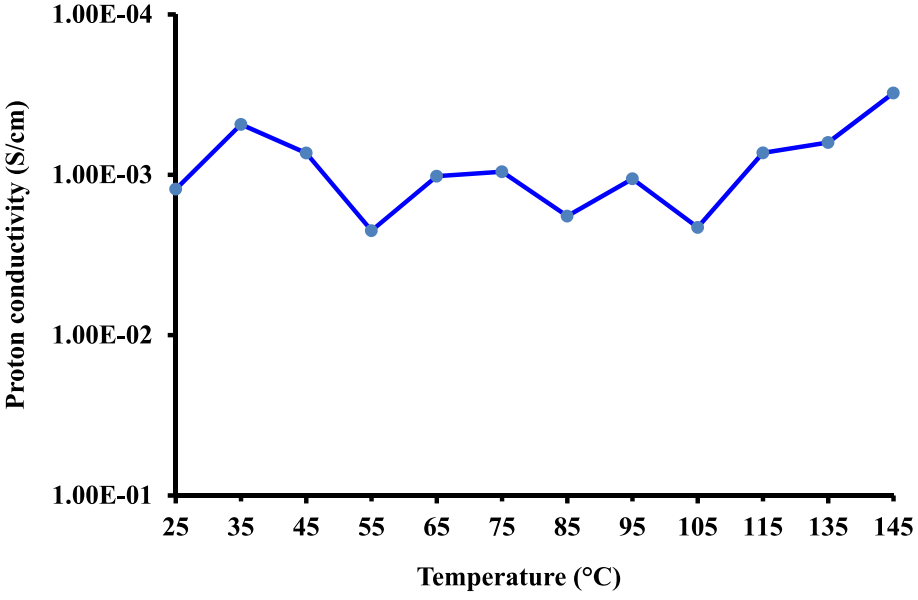


Fig. 3. Effect of different temperatures on the proton conductivity of the 8 wt% $ZrSiO_4$/PVDF membrane.

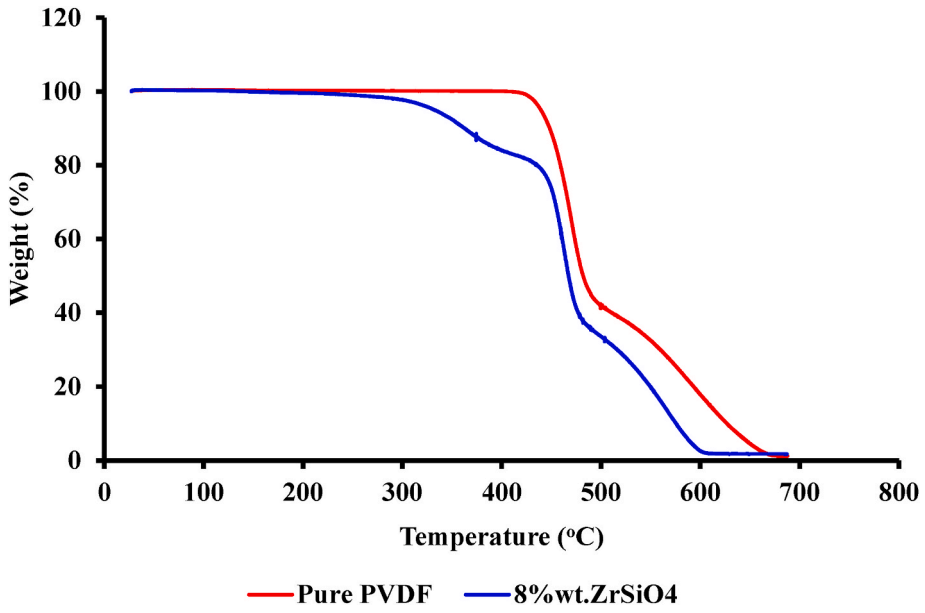


Fig. 4. TGA results for the compared membranes. Pure PVDF Vs the 8%wt. $ZrSiO_4$/PVDF membrane.

membrane, which exhibited degradation up to 680 °C.

3.3.3. *Fourier transform infrared spectroscopy*

Fig. 5 illustrates the FTIR spectra of both pure PVDF and the most conductive membrane (8 wt% $ZrSiO_4$/PVDF). Notably, both samples exhibited the presence of water molecules within their structures, as evidenced by sharp peaks in the range of 1685–1830 cm^{-1}, corresponding to H–*O*–H stretching of entrapped water molecules [31]. Additionally, characteristic peaks at 1070, 1168, and 1227 cm^{-1} were observed and explained by the stretching of CF_2 bonds. The peaks observed at 876 and 835 cm^{-1} were identified as one of PVDF's characteristic peaks, related to –CH stretching oscillations [47]. In the spectrum of 8 wt% $ZrSiO_4$, a notable increase in absorption was observed at these peaks, indicating larger stretching of the bonds due to the presence of $ZrSiO_4$ within the matrix. However, slight differences between the two spectra were observed. Specifically, two additional peaks at 1650 cm^{-1} and 1615 cm^{-1} were evident in the spectrum of membranes containing $ZrSiO_4$, absent in pure PDF. This occurrence was attributed to Si–O stretching vibration. Furthermore, vibrational stretching at 973 cm^{-1} demonstrates the presence of the Zr–Si bond [48].

3.3.4. *X-ray diffraction results*

The XRD spectrum shown in Fig. 6 for the $ZrSiO_4$ powder synthesized in the lab reveals characteristic peaks at 19.04°, 21.3°, 27.1°, and 39°, which correspond to specific crystallographic planes of monoclinic zirconium silicate. The peak at 19.04° aligns with the (110) plane, while 21.3° is associated with the (111) plane. The peak at 27.1° likely corresponds to the (200) plane and 39° is attributed to the (220) or (211) diffraction planes. These peaks confirm the crystalline nature of the $ZrSiO_4$ powder, which is consistent with the monoclinic structure. The observed diffraction patterns match the reference data from JCPDS Card No. 37–1484, confirming the material's phase and crystalline properties.

Similarly, in Fig. 7, the comparison of XRD patterns between pure PVDF and the 8 wt% $ZrSiO_4$/PVDF membrane, reveals significant differences in crystallinity and structure. The XRD analysis of the PVDF membrane revealed distinct peaks at 18.4°, 20.07°, 26.51°, 39.4°, and 41.75°, which correspond to the characteristic diffraction planes of the

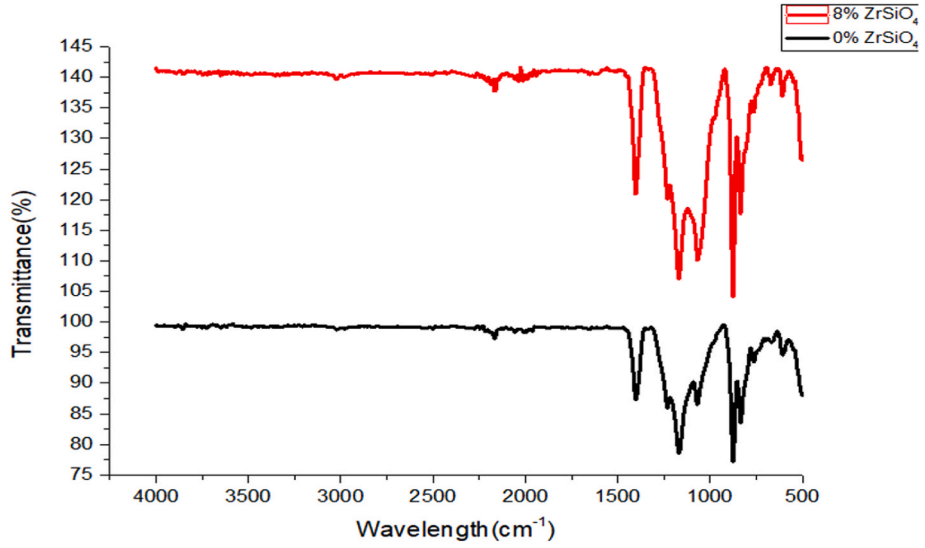


Fig. 5. FTIR Spectra of pure PVDF and 8 wt% $ZrSiO_4$/PVDF membrane.

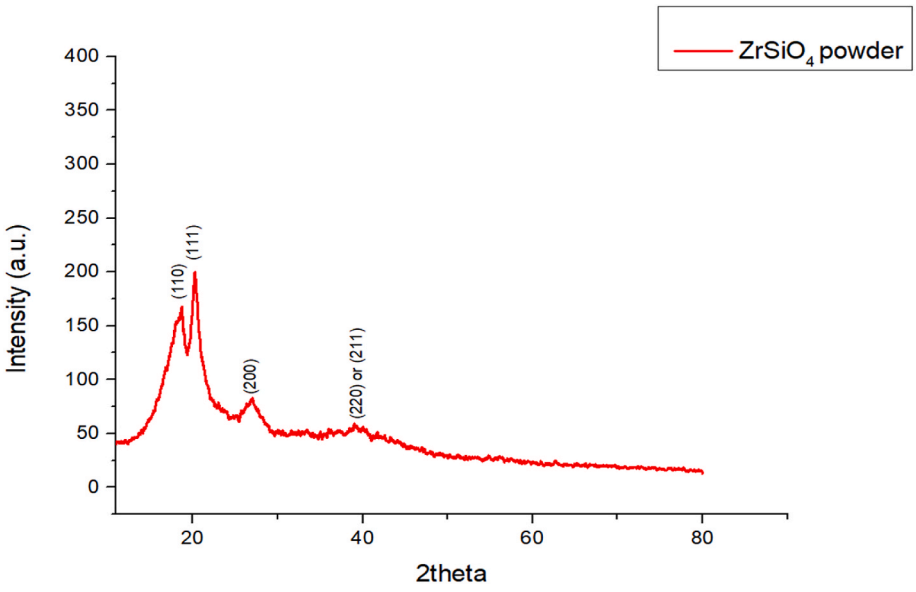


Fig. 6. XRD pattern for the synthesized $ZrSiO_4$ powder.

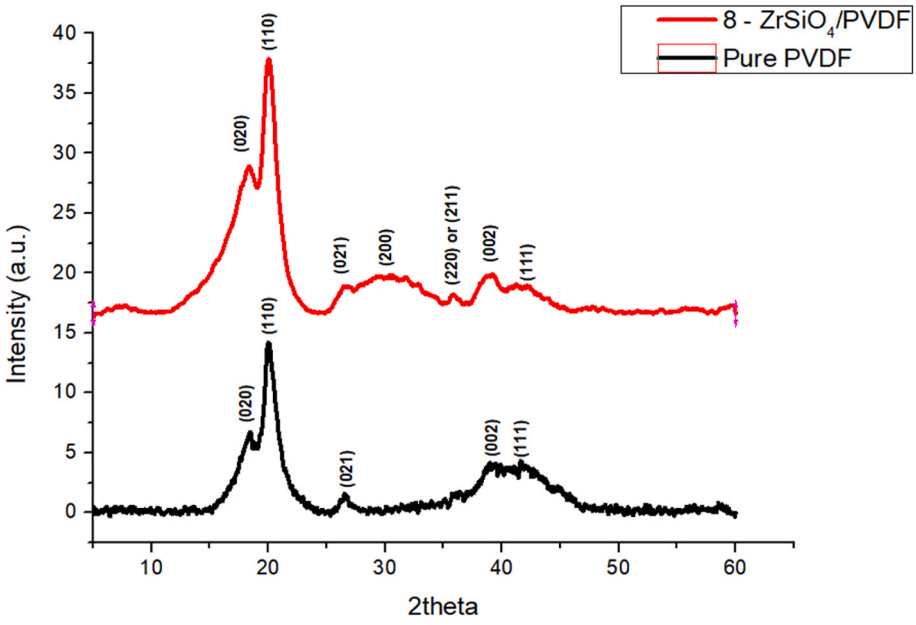


Fig. 7. XRD pattern of pure PVDF and 8 wt% $ZrSiO_4$/PVDF membrane.

α-phase. Specifically, the peaks at 18.4° and 20.07° are associated with the (110) and (020) planes, respectively, confirming the presence of the monoclinic α-phase structure. The additional peaks observed at 26.51°, 39.4°, and 41.75° further corroborate the semi-crystalline nature of α-phase PVDF, which is known for its mechanical robustness and thermal stability. These findings align with the reference patterns provided by the JCPDS database (Card No. 42–1650). Furthermore, the XRD pattern of the $ZrSiO_4$/PVDF composite revealed additional peaks at 30° and 35.8° 2θ, characteristic of zirconium silicate ($ZrSiO_4$). These peaks correspond to the (200) and (211 or 220) reflections of $ZrSiO_4$, indicating the successful incorporation of zirconium silicate into the PVDF matrix. The appearance of these additional peaks confirms the crystallization of $ZrSiO_4$ in the composite material and suggests a synergistic interaction between the PVDF polymer and $ZrSiO_4$, which may enhance the composite's properties. The presence of these peaks is consistent with known diffraction patterns of $ZrSiO_4$ (JCPDS Card No. 37–1484).

3.3.5. Scanning electron microscopy

Fig. 8 illustrates the morphology of the pure PVDF membrane, showing a smooth and dense surface with limited porosity. At lower magnifications, the membrane appears uniform, with only a few minor voids or defects, while higher magnifications reveal compact regions characteristic of PVDF's semi-crystalline structure [49]. In contrast, Fig. 9, which depicts the PVDF membrane modified with 8 wt% $ZrSiO_4$, reveals significant morphological changes. At lower magnifications (500× and 1,000x), the membrane exhibits interconnected spherical particles, indicating increased roughness due to the addition of $ZrSiO_4$. Higher magnifications (2,500× and 100,000x) show $ZrSiO_4$ particles embedded within the PVDF matrix, showing a layered configuration of very small particles (less than 500 nm). However, some agglomeration is still evident, particularly in regions where particles appear to cluster together rather than being well and evenly dispersed throughout the membranes' matrix. The inclusion of $ZrSiO_4$ enhanced the surface

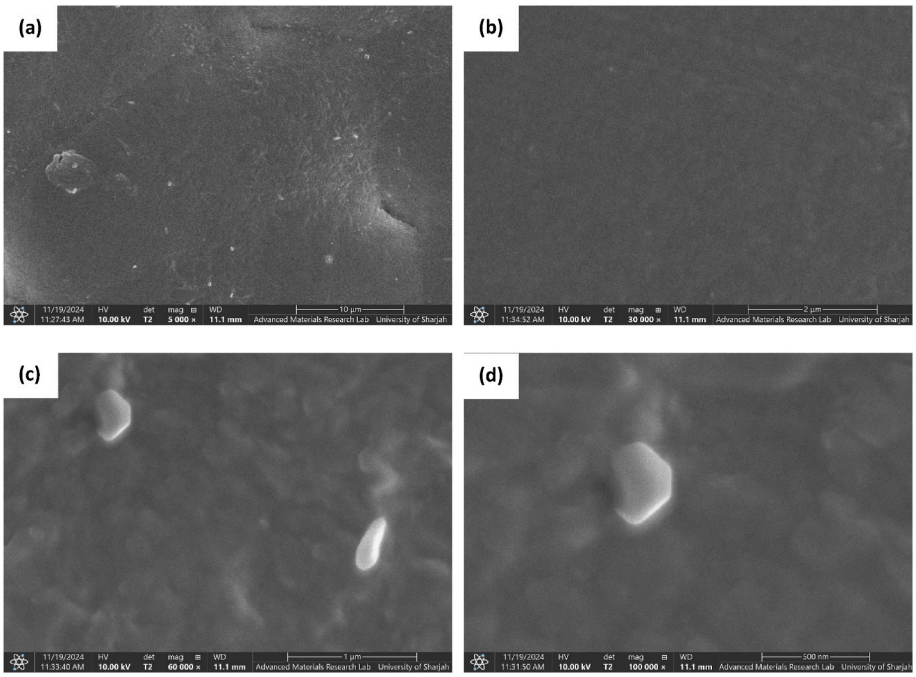


Fig. 8. SEM images of pure PVDF at the following magnifications: (a) 5000 × , (b) 30,000 × , (c) 60,000 × , and (d) 100,000 × .

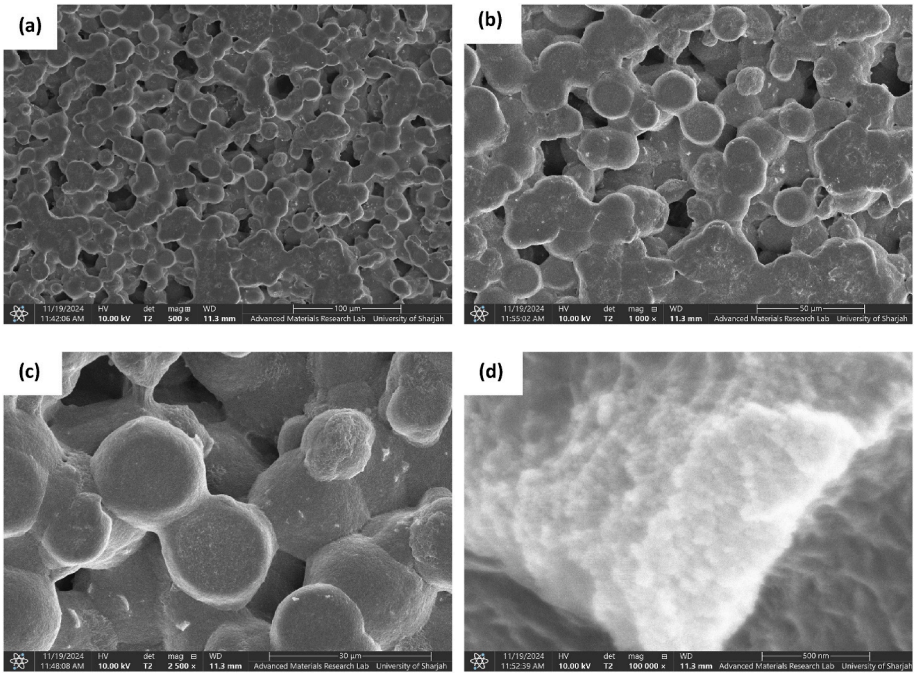
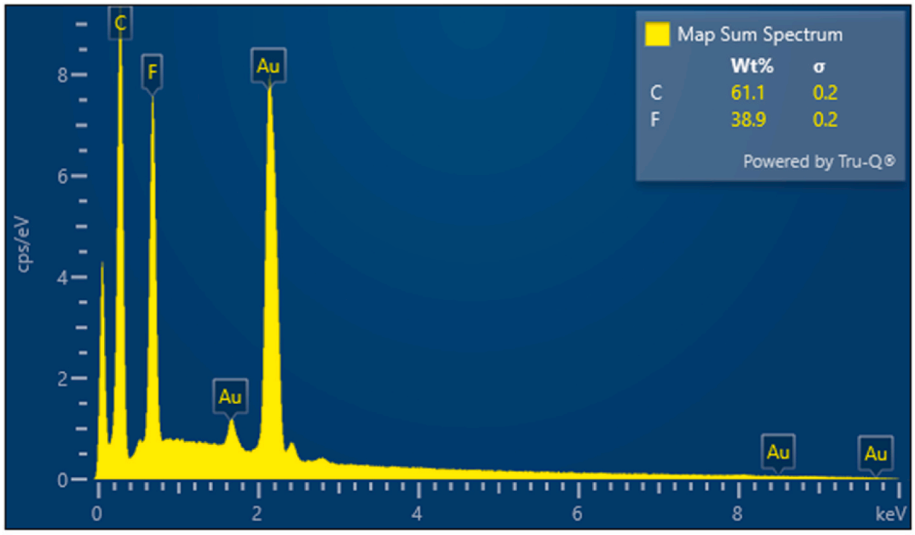


Fig. 9. SEM images of 8%wt.$ZrSiO_4$/PVDF membrane at the following magnifications: (a)500 × , (b)1000 × , (c)2500 × , (d) 100,000 × .

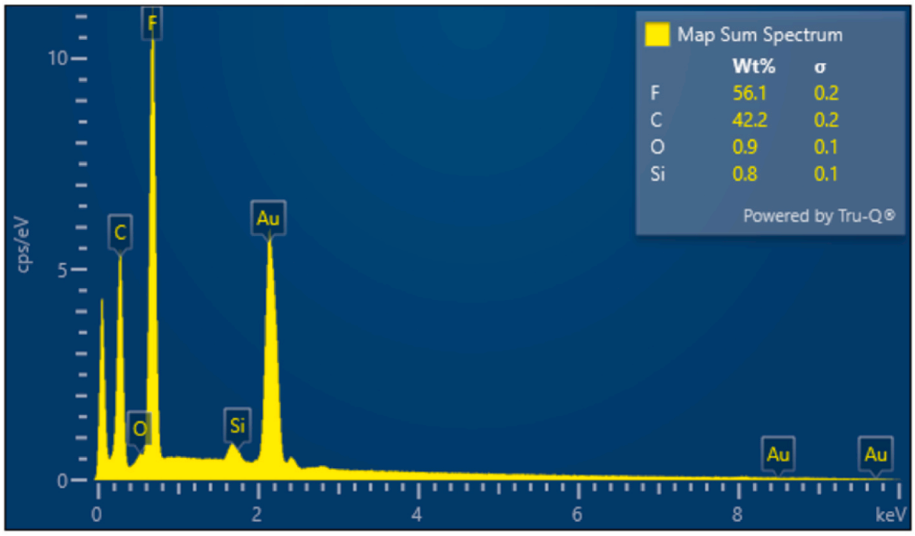
roughness and provided multiple surfaces for proton conduction. This has been positively reflected in proton conductivity values, and suitability for high-temperature PEMFCs. The agglomeration seen in SEM images suggests that further dispersion for the filler material in the PVDF membrane matrix is still required to achieve a more uniform membrane and to maintain the mechanical integrity. However, excessive agglomeration can affect the membranes' performance by creating pores and concentrated filler areas, which affect the mechanical properties and proton conduction paths. A proper dispersing agent is required in this case to ensure consistent properties across the membrane.

3.3.6. *Energy dispersion X-ray spectroscopy*

Fig. 10 (a) and (b) display the EDX spectrum of pure PVDF and the highest performing membrane, respectively. As observed in Fig. (a), the two dominant peaks of C and F confirm the membrane's composition as pure PVDF, consisting primarily of carbon and fluorine. The gold detected is from sputter coating and does not indicate contamination. The analysis aligns with expectations for a PVDF membrane, validating its elemental purity and preparation for imaging. In addition, the spectrum in Fig. 10 (b), also confirms the successful incorporation of $ZrSiO_4$ into the PVDF membrane, with the dominant peaks for fluorine (F) and carbon (C), highlighting PVDF as the primary component. Smaller peaks



(a)



(b)

Fig. 10. (a) EDX spectrum of the pure PVDF and (b) EDX spectrum of 8 wt% $ZrSiO_4$/PVDF membrane.

for oxygen (O) and silicon (Si) at 0.9 % and 0.8 % indicate the presence of $ZrSiO_4$ in the polymer matrix, consistent with its 8 wt% addition. The low intensity of the Si peak suggests $ZrSiO_4$ is present in small amounts, while gold (Au) peaks are attributed to sputter coating for SEM imaging. These results confirm the successful integration of $ZrSiO_4$, expected to enhance the membrane's thermal stability, porosity, and hydrophilicity, as supported by SEM analysis.

4. Conclusions

This work demonstrated a novel membrane composed of PVDF and zirconium silicate. The findings reveal a substantial enhancement in the membranes' conductivity with the incorporation of these materials, particularly notable with the addition of 8%wt. Of $ZrSiO_4$, resulting in a remarkable increase from 1.83×10^{-4} to 2.13×10^{-3} S/cm at 105 °C. This enhancement represents a significant advancement, showcasing a one-order-of-magnitude improvement in conductivity. Moreover, the membrane underwent characterization using water uptake test, FTIR, TGA, SEM, XRD, and EDS techniques to gain a comprehensive understanding of its morphology, structure, and thermal stability. Despite exhibiting lower thermal stability compared to pure PVDF, the new membrane demonstrated enhanced proton conductivity, thus highlighting its potential for use in high-performance applications. The FTIR analysis corroborated the presence of Zr–Si bonds within the membrane structure, providing further evidence of the successful incorporation of zirconium silicate. Moreover, the correlation between FTIR results and water uptake measurements offered valuable insights into the water content of these membranes, elucidating crucial aspects of their physicochemical properties. Overall, this research contributes to the growing body of knowledge surrounding composite membrane materials, offering a promising avenue for the development of advanced proton-conducting membranes. By leveraging the synergistic effects of PVDF and zirconium silicate, this membrane holds immense potential for applications in various fields.

CRediT authorship contribution statement

Tallah Magdi Ahmed: Writing – review & editing, Writing – original draft, Methodology, Investigation, Formal analysis, Data curation. **Amani Al Othman:** Writing – review & editing, Writing – original draft, Project administration, Methodology, Investigation, Funding acquisition, Formal analysis, Conceptualization. **Abdulrahim Shamayleh:** Writing – original draft, Project administration, Investigation, Funding acquisition, Conceptualization. **Muhammad Tawalbeh:** Writing – review & editing, Writing – original draft, Supervision, Project administration, Formal analysis, Data curation, Conceptualization.

Declaration of competing interest

The authors declare that they have no known competing financial interests or personal relationships that could have appeared to influence the work reported in this paper.

The authors declare no conflict of interest.

Acknowledgments

The authors acknowledge the financial support available from the American University of Sharjah through FRG22-C-E06 and Petrofac Endowed Chair Funds. They would like to thank the University of Sharjah, United Arab Emirates for financial support via the targeted research grant project number: 23020406306. The authors also acknowledge the support of the Advanced Materials Research Lab. at the University of Sharjah for the characterization of the materials used.

Data availability

Data will be made available on request.

References

[1] B. Zohuri, Hydrogen Energy, Springer International Publishing, Cham, 2019, https://doi.org/10.1007/978-3-319-93461-7.
[2] S. Maity, S. Sarkar, K. Dutta, T. De, R. Mukherjee, Renewable energy and green technology, in: Green Chemistry for Environmental Sustainability - Prevention-Assurance-Sustainability (P-A-S) Approach, IntechOpen, 2023, https://doi.org/10.5772/intechopen.1003716.
[3] P. Sharma, O.P. Pandey, Proton exchange membrane fuel cells: fundamentals, advanced technologies, and practical applications, in: PEM Fuel Cells, Elsevier, 2022, pp. 1–24, https://doi.org/10.1016/B978-0-12-823708-3.00006-7.
[4] M. Blal, A. Benatiallah, A. NeÇaibia, S. Lachtar, N. Sahouane, A. Belasri, Contribution and investigation to compare models parameters of (PEMFC), comprehensives review of fuel cell models and their degradation, Energy 168 (Feb. 2019) 182–199, https://doi.org/10.1016/j.energy.2018.11.095.
[5] T. Mkilima, et al., Carwash wastewater treatment through the synergistic efficiency of microbial fuel cells and metal-organic frameworks with graphene oxide integration, Case Studies in Chem. Environ. Eng. 9 (Jun. 2024) 100582, https://doi.org/10.1016/j.cscee.2023.100582.
[6] S. Sikder, Md M. Rahman, Efficiency of microbial fuel cell in wastewater (municipal, textile and tannery) treatment and bioelectricity production, Case Studies in Chem. Environ. Eng. 8 (Dec. 2023) 100421, https://doi.org/10.1016/j.cscee.2023.100421.
[7] M.A. Abdelkareem, K. Elsaid, T. Wilberforce, M. Kamil, E.T. Sayed, A. Olabi, Environmental aspects of fuel cells: a review, Sci. Total Environ. 752 (Jan. 2021) 141803, https://doi.org/10.1016/j.scitotenv.2020.141803.
[8] M. Bayat, S. Kaskun Ergani, Y. Daşdemirli, M. Kayfeci, Fuel cells basics and types, in: Handbook of Thermal Management Systems, Elsevier, 2023, pp. 371–399, https://doi.org/10.1016/B978-0-443-19017-9.00019-2.
[9] www.fortunebusinessinsights.com, "Fuel Cell Market Size, Share | Growth Analysis Report [2022-2030].".
[10] S. Ahmad, T. Nawaz, A. Ali, M.F. Orhan, A. Samreen, A.M. Kannan, An overview of proton exchange membranes for fuel cells: materials and manufacturing, Int. J. Hydrogen Energy 47 (44) (May 2022) 19086–19131, https://doi.org/10.1016/j.ijhydene.2022.04.099.
[11] N.M. Boyacioğlu, T. Kocakulak, M. Batar, A. Uyumaz, H. Solmaz, Modeling and control of a PEM fuel cell hybrid energy system used in a vehicle with fuzzy logic method, Int. J. Automo. Sci. Techno. 7 (4) (Dec. 2023) 295–308, https://doi.org/10.30939/ijastech..1340339.
[12] S. Dirkes, J. Leidig, P. Fisch, S. Pischinger, Prescriptive Lifetime Management for PEM fuel cell systems in transportation applications, Part II: on-board operando feature extraction, condition assessment and lifetime prediction, Energy Convers. Manag. 283 (May 2023) 116943, https://doi.org/10.1016/j.enconman.2023.116943.
[13] C. Zhang, Y. Zhang, L. Wang, X. Deng, Y. Liu, J. Zhang, A health management review of proton exchange membrane fuel cell for electric vehicles: failure mechanisms, diagnosis techniques and mitigation measures, Renew. Sustain. Energy Rev. 182 (Aug. 2023) 113369, https://doi.org/10.1016/j.rser.2023.113369.
[14] "Modelling and Design of PEM Fuel Cell Electric Military Armoured Vehicles Using a New Real-World Operation Profile model.".
[15] P. Xie, H. Asgharian, J.C. Vasquez, J. Guerrero, S.S. Araya, V. Liso, Day-ahead energy management for hybrid electric vessel with different PEM fuel cell modular configurations, Energy Rep. 9 (May 2023) 99–106, https://doi.org/10.1016/j.egyr.2022.12.091.
[16] Z. Wang, Z. Liu, L. Fan, Q. Du, K. Jiao, Application progress of small-scale proton exchange membrane fuel cell, Energy Rev. 2 (2) (Jun. 2023) 100017, https://doi.org/10.1016/j.enrev.2023.100017.
[17] S. Ahmad, T. Nawaz, A. Ali, M.F. Orhan, A. Samreen, A.M. Kannan, An overview of proton exchange membranes for fuel cells: materials and manufacturing, Int. J. Hydrogen Energy 47 (44) (May 2022) 19086–19131, https://doi.org/10.1016/j.ijhydene.2022.04.099.
[18] Y. Wang, D.F. Ruiz Diaz, K.S. Chen, Z. Wang, X.C. Adroher, Materials, technological status, and fundamentals of PEM fuel cells – a review, Mater. Today 32 (Jan. 2020) 178–203, https://doi.org/10.1016/j.mattod.2019.06.005.
[19] K. Ren, X. Liu, Z. Rao, Effect of temperature and external electric field on proton transport in ordered and amorphous proton exchange membranes: a molecular dynamics study, Int. J. Hydrogen Energy 54 (Feb. 2024) 1422–1435, https://doi.org/10.1016/j.ijhydene.2023.11.152.
[20] G.G. Gagliardi, O. Palone, E. Paris, D. Borello, An efficient composite membrane to improve the performance of PEM reversible fuel cells, Fuel 357 (Feb. 2024) 129993, https://doi.org/10.1016/j.fuel.2023.129993.
[21] M.A. Ziane, C. Join, M. Benne, C. Damour, N.Y. Steiner, M.C. Pera, A new concept of water management diagnosis for a PEM fuel cell system, Energy Convers. Manag. 285 (Jun. 2023) 116986, https://doi.org/10.1016/j.enconman.2023.116986.
[22] P. Kumar, R.P. Bharti, V. Kumar, P.P. Kundu, Polymer electrolyte membranes for microbial fuel cells: Part A. Nafion-based membranes, in: Progress and Recent Trends in Microbial Fuel Cells, Elsevier, 2018, pp. 47–72, https://doi.org/10.1016/B978-0-444-64017-8.00004-X.
[23] G. Xu, et al., Enabling high-temperature application of Nafion membrane via imitating ionic clusters in proton conduction channels, Int. J. Hydrogen Energy 56 (Feb. 2024) 330–337, https://doi.org/10.1016/j.ijhydene.2023.12.190.
[24] A.K. Sahu, S. Pitchumani, P. Sridhar, A.K. Shukla, Nafion and modified-Nafion membranes for polymer electrolyte fuel cells: an overview, Bull. Mater. Sci. 32 (3) (Jun. 2009) 285–294, https://doi.org/10.1007/s12034-009-0042-8.
[25] S. Moorthy, G. Sivasubramanian, D. Kannaiyan, P. Deivanayagam, Neoteric advancements in polybenzimidazole based polymer electrolytes for high-temperature proton exchange membrane fuel cells - a versatile review, Int. J. Hydrogen Energy 48 (72) (Aug. 2023) 28103–28118, https://doi.org/10.1016/j.ijhydene.2023.04.005.
[26] M. Kesava, V. Saravanan, S. Krishnan, K. Dinakaran, Lead(II) sulfide micro-crystals doped graphene nanosheets dispersed thermoplastic and multifunctional poly (benzoxazines) cured epoxy resin nanocomposites for medium temperature proton exchange membrane fuel cell applications, Polym. Adv. Technol. 34 (7) (Jul. 2023) 2153–2166, https://doi.org/10.1002/pat.6035.
[27] T. Senthil, P. Prabukanthan, D. Paradesi, K. Dinakaran, TiO $_2$ nanoparticle enhanced high temperature proton conductivity in hyperbranched sulfonated polyarylene aliphatic ketones for proton exchange membrane fuel cell applications, J. Appl. Polym. Sci. 140 (15) (Apr. 2023), https://doi.org/10.1002/app.53737.
[28] T. Senthil, A. Chandramohan, P. Senthil Kumar, D. Paradesi, K. Dinakaran, Proton-exchange membrane fuel-cell studies on composite films of Bi_2S_3 microrod-loaded random conjugated copolymer containing carbazole and diphenyl sulfone, Ind. Eng. Chem. Res. 62 (43) (Nov. 2023) 17743–17754, https://doi.org/10.1021/acs.iecr.3c02527.
[29] R. Al Shaikh, A. Al-Othman, M. Tawalbeh, A. Shamayleh, P. Nancarrow, Development of MXene incorporated PVDF based membranes for an enhanced performance in higher temperature PEM fuel cells, Process Saf. Environ. Protect. 189 (Sep. 2024) 985–994, https://doi.org/10.1016/j.psep.2024.06.126.
[30] Y. Lu, Y. Ma, T. Yang, J. Guo, Hydrophilic modification of PVDF membranes by *in situ* synthesis of nano-Ag with nano-ZrO_2, Green Process. Synth. 10 (1) (Aug. 2021) 538–546, https://doi.org/10.1515/gps-2021-0050.
[31] R.M. Nauman Javed, A. Al-Othman, P. Nancarrow, M. Tawalbeh, Zirconium silicate-ionic liquid membranes for high-temperature hydrogen PEM fuel cells, Int. J. Hydrogen Energy 52 (Jan. 2024) 894–908, https://doi.org/10.1016/j.ijhydene.2022.05.009.
[32] M. Tawalbeh, W. Nimir, A. Al-Othman, A. Ka'ki, High proton conduction in zirconium silicate/lignin/ionic liquids based- membranes for high temperature PEM fuel cells, Process Saf. Environ. Protect. 190 (Oct. 2024) 779–791, https://doi.org/10.1016/j.psep.2024.07.094.
[33] A.M. Abdelkader, A. Daher, E. El-Kashef, Novel decomposition method for zircon, J. Alloys Compd. 460 (1–2) (Jul. 2008) 577–580, https://doi.org/10.1016/j.jallcom.2007.06.032.
[34] T. Gayathri, N. Kavitha, A. Chandramohan, D. Roy, K. Dinakaran, Mesoporous zirconia nanostructures embedded Polyvinyledine difluoride conducting films for EMI shielding applications, Mater. Today Proc. 59 (2022) 534–539, https://doi.org/10.1016/j.matpr.2021.11.564.

[35] H. Sepehrian, A.R. Khanchi, M.K. Rofouei, S. Waqif Husain, Non-thermal synthesis of mesoporous zirconium silicate and its characterization, J. Iran. Chem. Soc. 3 (3) (Sep. 2006) 253–257, https://doi.org/10.1007/BF03247216.
[36] M. Trulsson, B. Jönsson, C. Labbez, On the origin of the halo stabilization, Phys. Chem. Chem. Phys. 15 (2) (2013) 541–545, https://doi.org/10.1039/C2CP42404E.
[37] A. Al-Othman, et al., Novel composite membrane based on zirconium phosphate-ionic liquids for high temperature PEM fuel cells, Int. J. Hydrogen Energy 46 (8) (Jan. 2021) 6100–6109, https://doi.org/10.1016/j.ijhydene.2020.02.112.
[38] A. Amalorpavadoss, N. Kavitha, A. Chandramohan, P. Santhiya, K. Dinakaran, Synthesis and characterization of piperazine containing polyaspartimides blended polysulfone membranes for fuel cell applications, J. Solid State Electrochem. 25 (4) (Apr. 2021) 1421–1431, https://doi.org/10.1007/s10008-021-04924-y.
[39] J. Pandey, F.Q. Mir, A. Shukla, Synthesis of silica immobilized phosphotungstic acid (Si-PWA)-poly(vinyl alcohol) (PVA) composite ion-exchange membrane for direct methanol fuel cell, Int. J. Hydrogen Energy 39 (17) (Jun. 2014) 9473–9481, https://doi.org/10.1016/j.ijhydene.2014.03.237.
[40] J.W. Lee, et al., Synthesis and characterization of acid-doped polybenzimidazole membranes by sol–gel and post-membrane casting method, J. Membr. Sci. 357 (1–2) (Jul. 2010) 130–133, https://doi.org/10.1016/j.memsci.2010.04.010.
[41] S.S. Alrwashdeh, A.M. Al-Falahat, H. Markötter, I. Manke, Visualization of water accumulation in micro porous layers in polymer electrolyte membrane fuel cells using synchrotron phase contrast tomography, Case Studies in Chem. Environ. Eng. 6 (Dec. 2022) 100260, https://doi.org/10.1016/j.cscee.2022.100260.
[42] M. Kesava, K. Dinakaran, SnO $_2$ nanoparticle assisted enhanced proton exchange membrane fuel cell performance of sulfuric acid-doped porous poly (Triphenylpyridine–Aliphatic ethers), J. Phys. Chem. C 125 (1) (Jan. 2021) 130–142, https://doi.org/10.1021/acs.jpcc.0c08739.
[43] M. Kesava, K. Dinakaran, SnO2 nanoparticles dispersed carboxylated Poly(arylene ether sulfones) nanocomposites for proton exchange membrane fuel cell (PEMFC) applications, Int. J. Hydrogen Energy 46 (1) (Jan. 2021) 1121–1132, https://doi.org/10.1016/j.ijhydene.2020.09.178.
[44] Y. Yin, et al., Enhanced proton conductivity of Nafion composite membrane by incorporating phosphoric acid-loaded covalent organic framework, J. Power Sources 332 (Nov. 2016) 265–273, https://doi.org/10.1016/j.jpowsour.2016.09.135.
[45] P. Sharma, O.P. Pandey, Proton exchange membrane fuel cells: fundamentals, advanced technologies, and practical applications, in: PEM Fuel Cells, Elsevier, 2022, pp. 1–24, https://doi.org/10.1016/B978-0-12-823708-3.00006-7.
[46] A.J. de Jesus Silva, M.M. Contreras, C.R. Nascimento, M.F. da Costa, Kinetics of thermal degradation and lifetime study of poly(vinylidene fluoride) (PVDF) subjected to bioethanol fuel accelerated aging, Heliyon 6 (7) (Jul. 2020) e04573, https://doi.org/10.1016/j.heliyon.2020.e04573.
[47] H. Bai, X. Wang, Y. Zhou, L. Zhang, Preparation and characterization of poly (vinylidene fluoride) composite membranes blended with nano-crystalline cellulose, Prog. Nat. Sci.: Mater. Int. 22 (3) (2012) 250–257.
[48] V.V. Avdin, I.V. Krivtsov, A.A. Lymar, Yu V. Matveichuk, Structure formation of the mixed gels of zirconium oxyhydrate and silicic acid produced with different sequencing of reagents, J. Struct. Chem. 52 (6) (Dec. 2011) 1172–1178, https://doi.org/10.1134/S0022476611060242.
[49] A. Huang, C. Dong, Y. Gao, L. Liu, X. Yan, P. Yin, Supramolecular complexation of metal oxide clusters in PVDF-PVP blends for large scale fabrication of proton exchange membranes for fuel cells, Polymer (Guildf) 299 (Apr. 2024) 126951, https://doi.org/10.1016/j.polymer.2024.126951.